2021-02

Enhancing the performance of a spray flash evaporation integrated with evacuated tube desalination system

Muhunzi, Amour

NM-AIST

https://doi.org/10.58694/20.500.12479/1298

ENHANCING THE PERFORMANCE OF A SPRAY FLASH EVAPORATION INTEGRATED WITH EVACUATED TUBE DESALINATION SYSTEM

Amour Othman Muhunzi

A Dissertation Submitted in Partial Fulfillment of the Requirements for the Degree of Master's in Sustainable Energy Science and Engineering of the Nelson Mandela African Institution of Science and Technology

Arusha, Tanzania

February, 2021

ABSTRACT

Numerical analysis for heat exchanger for spray-assisted low-temperature desalination system is presented for an existing low-temperature desalination unit at Arusha Technical College (ATC). The current desalination unit at ATC has two suction fans and a water pump in the condensation unit where significant amount of energy is consumed. So, it will be impractical to implement such a type of desalination system in remote areas where there is limited access to electricity. The study aims to come up with a suitable model for the replacement of the current condensation unit due to high energy consumption. The heat transfer phenomena have been analyzed to understand the effect of mass flow rate, tube length and diameter in a shell-and-tube heat exchanger (STHX). A Math CAD model was developed using the Delaware method to obtain the mentioned parameters. The results show that the pressure drop is very low from all STHX configurations, while the heat transfer coefficient seems to be maximum in the smallest diameter within the largest tube length heat exchanger. The maximum possible energy will be extracted by the STHX from the steam while it condenses. According to the results, as long as over-design is considered the proposed system can be implemented with the minimum effect of 5.968 to 10.688 kWh energy consumption. The energy-saving of the proposed system is about 8.856 kWh as the replacement of the STHX from the existing condensation unit. While the current system energy is consumed about 14.824 to 19.544 kWh in a single day of operation. Also, the proposed system will improve the system workability to the remote communities in future implementation.

DECLARATION

I, Amour Othman Muhunzi do hereby declare to the Senate of The Nelson Mandela African Institution of Science and Technology that this dissertation is my original work and that it has neither been submitted nor being concurrently submitted for degree award in any other institution.

Amour Othman Muhunzi

03/04/2021

Name and signature of candidate **Date**

The above declaration is confirmed

Dr. Yusufu Abeid Chande Jande

03/04/2021

Name and signature of principal supervisor **Date**

Prof. Revocatus Lazaro Machunda

03/4/2021

Name and signature of co-supervisor **Date**

COPYRIGHT

CERTIFICATION

The undersigned, certify that they have read and hereby recommend for acceptance by The Nelson Mandela African Institution of Science and Technology a dissertation entitled *"Enhancing the Performance of a Spray Flash Evaporation Integrated with Evacuated Tube Desalination System"* to be accepted in partial fulfillment of the requirements for the degree of Master's in Sustainable Science and Engineering of the Nelson Mandela African Institution of Science and Technology, Arusha, Tanzania.

Dr. Yusufu Abeid Chande Jande

Yjande

03/04/2021

Principal supervisor **Date**

Prof. Revocatus Lazaro Machunda

03/4/2021

Co-supervisor **Date**

ACKNOWLEDGEMENTS

It would not be possible without the blessings of Almighty Allah who is creator, sustainer, nourisher, pillar, understanding, knowledge, wisdom, source of inspiration and strength throughout this program. The author would like to gratitude his family members whose encouragement has made sure that gave it all it takes to finish that which has been started. The author expresses his earnest gratitude to beneficial supervisors Dr. Yusufu Abeid Chande Jande and Prof. Revocatus Lazaro Machunda for their intensive support. Also, he is so grateful to Dr. Sam Otukol for allowing him to perform this study. Lastly, the author would like to convey a special thanks to the whole community members who have been affected in every way possible by this quest.

DEDICATION

This work is lovely dedicated to my mother (my camaraderie/hero).

TABLE OF CONTENTS

LIST OF TABLES

LIST OF FIGURES

LIST OF ABBREVIATIONS AND SYMBOLS

CPC	Compound Parabolic Concentrator
ED	Electro-Dialysis
GHG	Greenhouse Gases
LFR	Linear Fresnel Reflector
MED	Multi-Effect Distillation
MSF	Multi-Stage flash
PTC	Parabolic Trough Collector
RO	Reverse Osmosis
STHX	Shell and Tube Heat Exchangers
VC	Vapor Compression
A	Area (m^2)
Cp	Specific Heat Capacity (kJ/kg)
D,d	Diameter (m)
Ft	Correction Factor
ft	Darcy Friction Factor
G	Mass Velocity (kg/s m^2)
h	Heat Transfer Coefficient (W/m^2 K)
k	Thermal Conductivity (W/m K)
ṁ	Mass flow Rate (kg/s)
n	Pass Number, Number
Pr	Prandtl Number
Q	Heat Load (kW)
Re	Reynold Number
s	Specific Gravity
t	Temperature (˚C)
U	Overall Heat Transfer Coefficient (W/m^2 K)
μ	Viscosity (kg/m s)
ρ	Density (kg/m^3)
ΔP	Pressure Drop (Pa)
ΔT	Temperature Difference (K)
b	Baffle
c	Clearance, Clean

d	Design
e	Equivalent
f	Liquid, Cold Fluid
g	Vapour, Gas, Steam
i	Initial, Inner
lm	Logarithmic Mean
m	Material, Mean
n	Nozzles
o	Outer
r	Return
req	Required
s	Shell
t	Tube
w	Water

Subscripts Numbers

2	Cold Fluid Inlet
3	Cold Fluid Outlet
6	Hot Fluid Inlet
7	Hot Fluid Outlet

CHAPTER ONE

INTRODUCTION

1.1 Background of the Problem

The present society demands the efficient utilization of energy and at the same time reducing environmental impact to contribute to sustainable economic development. More freshwater consumption is caused by the development of the world industry and human population growth (Chen *et al*, 2018b). Desalination of brackish water or seawater is an important approach to solve the water resource dearth. The reverse osmosis (RO), electro-dialysis (ED), vapor compression (VC), multi-effect distillation (MED) and multi-stage flash (MSF) desalination technologies are more popular, which most of them are conventionally operated by fossil fuels that contribute to greenhouse gas (GHG) emissions. However, the researchers have come up with the idea of using renewable energy such as ocean thermal energy conversion (OTEC), wind and solar energy as an alternate means of fueling desalination units (Ikegami *et al.*, 2006). Desalination processes that are assisted by solar energy are not yet commercialized; small capacity desalination plants that utilize solar PV and wind energy have been invented to serve the remote communities (Herrero-Gonzalez *et al.*, 2018).

Sometimes using low-grade waste heat for desalination and the combined fossil fuel and solar desalination could be more cost-effective (Li *et al.*, 2013). This attracted researchers' invention and innovation on low-temperature and low-pressure desalination system that it simply agree to use low-grade heat. By considering the reduction of heat losses to the surroundings, the higher collection efficiency, low-cost glass flat plate solar collectors with temperatures up to 80°C have been used (Siddique *et al.*, 2018). Moreover, the spray flash evaporation desalination has been used for more than four decades due to the liquid jet which improves the rate of flash evaporation compared to superheated pool water and superheated liquid in conventional MSF evaporators (Miyatake *et al.*, 1981). The level of jet shattering is strongly causing more violent and faster evaporation in flash evaporator related to the superheat degree (Mutair & Ikegami, 2009). The costs of energy consumption increased when the production of freshwater increased; the low energy efficiency is partly influencing the high cost of water production. The recovery ratio gained output ratio, and freshwater productivity rate are the factors that determine the performance of the desalination plant (Ahmed *et al.*, 2018). Many of the conventional spray flash evaporation use solar still aimed at preheating water before entering the evaporation chamber.

An extensive mathematical and experimental study on spray flash evaporation phenomena was conducted by Chen *et al.* (2018). The study specifically discussed a hot water jet sprayed into a low-pressure evaporator as applied by Muthunayagam *et al.* (2005). Araghi and Khiadani (2018) reported on dynamic thermo-fluid behavior and performance by utilizing a gas-liquid ejector in single-stage vacuum spray flash desalination. Miyatake *et al.* (1985) made an injection of bubble nuclei to enhancement the efficiency of spray flash evaporation, through investigating effects of superheating and nozzle diameter (Miyatake *et al.*, 1981), a liquid temperature (Miyatake *et al.*, & Yuda *et al.*, 1981), liquid flow rate, and electrolytic effects in the evaporator. El-Fiqi *et al.* (2007), and Mutair and Ikegami (2010) mainly investigated on flash evaporation characteristics from superheated water jets. Based on droplet analysis Cai *et al.* (2018) modeled the diffusion-controlled evaporation on the spray flash evaporator. Qian and Chua (2018) and Maria *et al.* (2016) carried out a detailed review of the thermodynamic model and mathematical modeling developed to precisely predict the performance of spray evaporator. Qi *et al.* (2018) analyzed the setting of the flash recovery system and optimize the design of flash chamber. Ja *et al.* (2018b) and El-Agouz *et al.* (2014) evaluated spray-assisted low-temperature desalination power by solar through numerical modeling. Ikegami *et al.* (2006) performed an experimental study on how much the direction of injection influences flash evaporation. Mutair and Ikegami (2009) investigated the formulation of correlation and influencing factors from superheated water jets on flash evaporation. Stengler *et al.* (2018) analyzed the function of low-pressure drop vertical gas-liquid separator together with a flash evaporator.

The effective energy utilization for sustainable economic development is demanded to reduce freshwater scarcity through the desalination technique, whereas the conventional desalination approach uses fossil fuels or sometimes combines with renewable energy souses. The low-grade waste heat combined with fossil fuels and solar provides cost-effective, while the solar collectors used in preheating saline water before entering into the evaporator. The liquid jet improves the rate of flash evaporation compared to superheated pool water which reduces the cost of water production. Also, the hot water jet sprayed into a low-pressure evaporator or a single-stage vacuum spray flash desalination which does not receive passive solar energy. Moreover, some of the literature was based on droplet analysis, characteristics of superheated water jets, diffusion-controlled evaporation, predict the performance of spray evaporator, the influence of the direction of injection, the flash recovery system and optimize the design of flash chamber and others, but don't directly explain the condensation unit if it is a separate unit in the spray flash evaporation desalination plant. Presently, Arusha Technical College (ATC)

has established a low-temperature desalination unit that consumes about 14.824-19.544 kWh in a single day of operation; especially in the condensation unit that comprises two suction fan and a water pump which consume about 8.856 kWh, even though it is a vital part of flash evaporation desalination technology. Hence, this research purely focuses on optimizing the condensation unit by replacing it with shell-and-tube heat exchanger through a numerical analysis.

1.2 Statement of the Problem

In the above literature, the flash evaporator has been reported from many theoretical and experimental studies as an essential unit in the low-temperature desalination technology. But there is no specific study that discusses the condensation unit on flash evaporation desalination technology. Moreover, currently, there is an existing low-temperature desalination unit at ATC, which uses 8.856 kWh energy at the condensation unit. Thus, this research is on enhancing the performance of a spray-assisted low-temperature desalination system by optimizing the condensation unit by replacing it with shell-and-tube heat exchanger. The heat exchanger is designed to reduce the level of energy consumption, allows a smooth working environment of the desalination unit.

1.3 Rationale of the Study

The present society demands the efficient utilization of energy and at the same time reducing environmental impact to contribute to sustainable economic development. More freshwater consumption is caused by the development of the world industry and human population growth (Chen *et al.,* & Chua, 2018b). Desalination of brackish water or seawater is an important approach to solve the water resource dearth. The reverse osmosis (RO), electro-dialysis (ED), vapor compression (VC), multi-effect distillation (MED) and multi-stage flash (MSF) desalination technologies are more popular, which most of them are conventionally operated by fossil fuels that contribute to greenhouse gas (GHG) emissions. The low-grade waste heat combined with fossil fuels and solar provides cost-effective, while the solar collectors used in preheating saline water before entering into the evaporator. Since the evaporation chamber is made of glass material and receives direct sun rays (passive solar), the use of a spray flash evaporation integrated with the evacuated tube desalination system is essential in developing sustainable sources of freshwater that consume low energy.

1.4 Research Objectives

1.4.1 Main Objective

To enhance the performance of a spray flash evaporation integrated with an evacuated tube desalination system.

1.4.2 Specific Objectives

(i) To optimize the condensation unit by replacing it with a shell-and-tube heat exchanger (STHX).

(ii) To scrutinize the effect of some parameters and configuration on the spray flash evaporator performance.

(iii) To assess the heat transfer phenomena due to mass flow rate, tube length and diameter in the design of STHX.

1.5 Research Questions

(i) To what extent the energy consumption could be reduced if the condensation unit by replacing with the STHX in the spray flash desalination unit installed at ATC?

(ii) For how much is STHX affect the current configuration and parameters on the spray flash evaporator performance?

(iii) What are the exact heat transfer phenomena due to variation of mass flow rate, tube length and diameter in the design of STHX?

1.6 Significance of the Study

The effective energy utilization for sustainable economic development is demanded to reduce freshwater scarcity through the desalination technique, whereas the conventional desalination approach uses fossil fuels or sometimes combines with renewable energy souses. In the aspects of energy consumption reduction for desalination, there are still improvement opportunities and ample research due to the huge desalination benefits as Tanzania has enough potential water bodies for increasing freshwater resources and improving water quality. Optimization of the energy consumption in the desalination system will attract government

and other stakeholders to invest, especially for remote communities, suitable small-scale desalination units.

1.7 Delineation of the Study

This study had focused on the design of the STHX to be used by the solar-driven desalination plant installed at ATC. Therefore, this research had focused on developing only one main part (shell-and-tube heat exchanger) of the evaporation desalination system to lower energy consumption for the current system.

CHAPTER TWO

LITERATURE REVIEW

2.1 Solar Assisted Desalination System

There are two main techniques to collect solar energy, direct use of the thermal energy from solar radiation through the solar collector and electrical power transferred from solar radiation through photovoltaic (PV) materials (Ruzhu & Ge, 2016). It is an advantage to desalination industries to utilize solar energy through solar PV panels and thermal collectors which are capable to make greener desalination industry (Sharon & Reddy, 2015). Instead of an electric heater, the solar collector has been used in preheating inlet water to minimize the electric energy consumption by the desalination system as shown in Fig. 1 and Fig. 3. Investigations on the integration of solar thermal collectors with desalination systems have been reported in different works and observed that the distillation capacity of the system is enhanced; and the overall efficiency of the system reaches the value of 67.6% (Rajaseenivasan & Srithar, 2017).

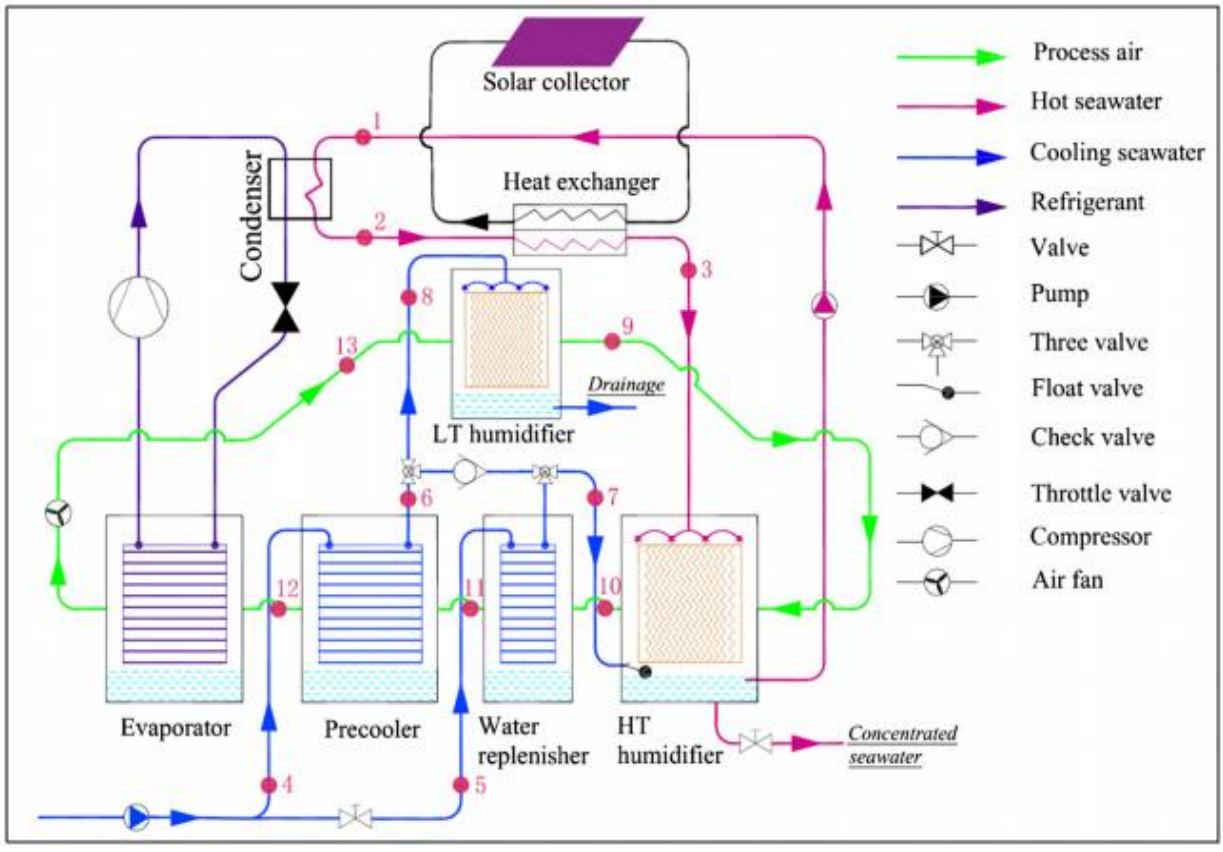

Figure 1: Illustration of the solar-assisted desalination system (Xu & Dai, 2019)

2.2 Solar Thermal Collector

Convenient drawing materials and simple structure are the key merits of the basin-type solar still to be widely used as a good example of the passive solar desalination system. Currently the studies on the basin-type still primarily concentrate on integrating with other solar thermal collectors, thermal performance improvements, and new materials drawing (Zheng, 2017). Depending on the solar radiation, less than 5 kg/m^2/d daily water output and nearby 30-45% the basin-solar still efficiency was reported by Hou *et al.* (2018). Low water productivity is the main drawback basin-type still in comparison to conventional methods (El-Agouz *et al.*, 2014). Noted from He and Yan (2009) that the operating efficiency of solar stills was low; mainly due to condensation that takes place in the basin and making difficult the evaporation temperature to raise, while the latent heat of condensation is released to the ambient. From the literature, there are three main types of solar thermal collectors: concentrated parabolic collector, evacuated tube collector and flat plate collector (Khan *et al.*, 2018). Evacuated tube collectors are made up of transparent glass tubes in one or many rows mounted on a frame. In diffuse or overcast sunlight conditions they are capable of high thermal efficiency close to that of bright sunshine (Mahbubul *et al.*, 2018) and indicative temperature 50-200^{o}C as appeared in Table 1. Evacuated tube collectors have noted to perform well when integrated with different solar desalination systems on improving the desalinated water production rate and efficiency of the system (Rahimi-Ahar *et al.*, 2018) as shown in Fig. 2.

Table 1:Solar thermal collector (Wang *et al.*, 2016)

Collector	Motion	Absorber type	Concentration ratio	Indicative temperature (^{o}C)
Flat plate	Stationary	Flat	1	30-80
Evacuated tube	Stationary	Flat	1	50-200
CPC	Stationary	Tubular	1-5	60-240
PTC	Single-axis tracking	Tubular	15-45	60-300
LFR	Single-axis tracking	Tubular	10-40	60-250
Parabolic dish	Two-axes tracking	Point	100-1000	100-500
Solar tower	Two-axes tracking	Point	100-1500	150-2000

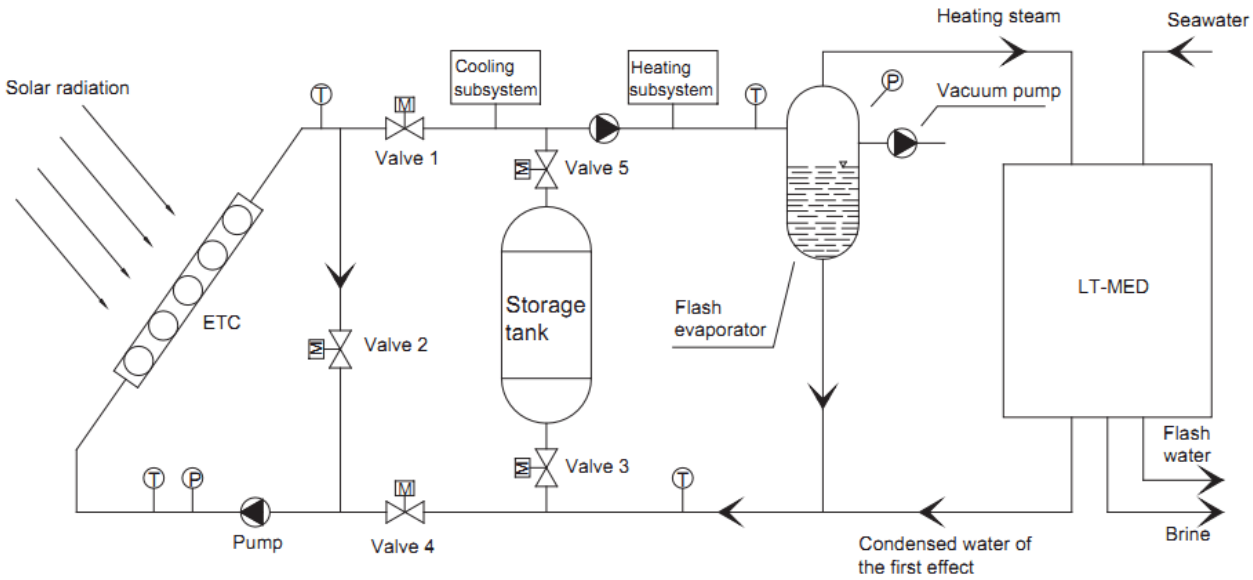

Figure 2: Flow chart of evacuated tube collectors desalination system (Liu *et al.*, 2013)

2.3 Spray Assisted Low-Temperature Desalination

Figure 3 shows a diagram of spray assisted low-temperature phase-change desalination technique which is the thermal-based method that makes no boundary upon heat and mass transfer mechanism and eliminates the contribution of mechanical energy input (Chen *et al.*, 2018a). A spray is a process whereby small droplets from continuous phase liquid disintegrated and dispersed into surrounding via a spray nozzle (Zhao *et al.*, 2018). When the surrounding saturation vapor temperature is slightly lower than that of the liquid stream injected into a low-pressure chamber will split into fine droplets (Chen *et al.*, 2018). Renewable energy sources integration with thermal desalination systems can be adapted through different concepts necessary in lowering energy consumption (Wellmann *et al.*, 2015). With lower initial cost, lower fouling and scaling potential, the simplicity of system design, and high heat and mass transfer rates made the spray assisted low-temperature desalination useful compared to the traditional thermal desalination technologies (Qian & Chua, 2018). This technology comprises two main units to reach the freshwater namely the evaporation unit and condensation unit (Gude & Nirmalakhandan, 2009). Fortunately, solar energy can either be used directly or indirectly to supply thermal energy to an evaporation unit to produce steam (Al-Kharabsheh & Yogi, 2003). However, the heat exchange process occurs in the condensation unit by exchanging steam temperature with that of cooling media (gas or liquid) and condensing the steam into liquid water (Roy, 2018).

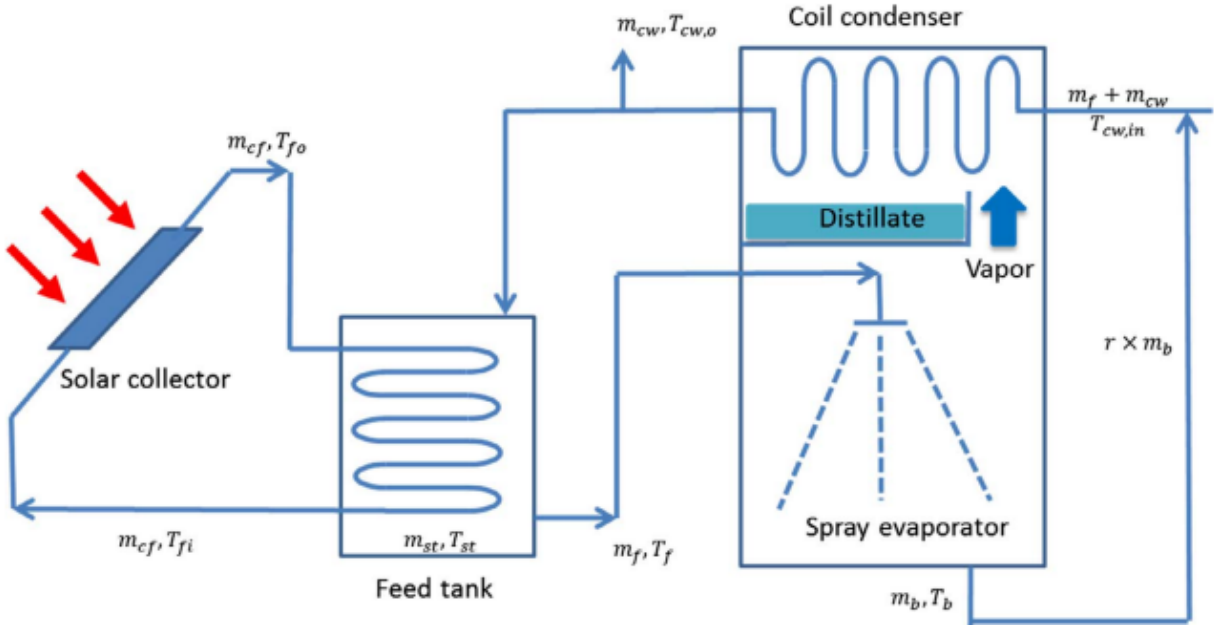

Figure 3: Illustration of the spray-assisted low-temperature desalination (Ja *et al.*, 2018b)

2.4 Shell-and-Tube Heat Exchanger

Heat exchange refers to the process which takes place between channels/medium when there is a temperature gradient between them. The heat exchange process occurs when fluids of the channels exchange their temperature by passing through a heat exchanger (Sundén & Manglik, 2007). The heat exchanger is a device or a structure that permits heat transfer, and often goes together with mass transfer. Heat exchangers vary in size, shape, transfer mode, and other features depending on the performance characteristics, construction, and application (Thulukkanam, 2013). They have been used in various industries including process industries, power plants, chemical, pharmaceutical, petrochemical, and engineering (Arani & Moradi, 2019). To avoid equipment failure and undesired operations, the selection of appropriate configuration for a specific process is vital. Various tubular heat exchanger categories including STHX, double-pipe, and spiral-tube heat exchanger; and they have been used in various heating and cooling devices (Kakaç *et al.*, 2002). Among the categories, STHX models are the best and extensively used (Nitsche & Gbadamosi, 2015). The STHX uses indirect contact mode exchangers where heat is exchanged in a transient manner (Bichkar *et al.*, 2018). One fluid stream flows on the shell across or along the tubes whereas the other flows through tubes. In STHX corrosive fluid should pass through tubes while non-corrosive one passes through the shell, whereas only the channels, heads, tubes, and tube-sheets will need expensive corrosion-resistant alloys. The STHX provides a great heat transfer area to weight and volume. Also, they could be simply constructed in an extensive range of sizes in comparison with other categories of heat exchanger (Ambekar *et al.*, 2016).

The STHX comprises tubes, tube sheets or shell, baffles, rear-end and front-end head as the essential parts, and they have been designed in a range of different inner constructions, depending on the anticipated heat transfer and pressure drop performance. The most common design of STHX is U-tube design, fixed tube sheet design, and floating head type. All the designs are subjected to thermal stresses in the tube, tube sheet, the front-end head which are always fixed, whereas the rear-end head can either be fluctuating or fixed, due to variation of temperature from heat transfer characteristics. The exchangers could operate with identical phases (gas or liquid) on each side that is identified as single-phase, or with two-phase as used in vaporization of liquid into a vapor or in condensing the vapor into a liquid with the phase transformation (Roy, 2018).

Currently, the minimum pressure drop with a greater coefficient of heat transfer is vital for the industries as an effective better condensation unit design (Solanki & Kumar, 2018). However, some of the literature has been studied on the design and optimization of STHX by introducing different types, amount and size of fluid molecules. Thakur *et al.* (2018) injected air bubbles at tube inlet for different Al_2O_3 nanoparticle concentrations and studied the heat transfer characteristics. The results show that the increase in air bubble injection and Al_2O_3 nanoparticle concentration, causes the increase of heat transfer coefficient and overall heat transfer coefficient. Another study done by Somasekhar *et al.* (2018) used fluent computational software to analyze distilled water, pressure drop characteristics and heat transfer of Al_2O_3 water nanofluid. The result shows an improvement in heat transfer characteristics when adding nanoparticles. Pahamli *et al.* (2016) evaluated Paraffin RT50 as phase change material based on thermal behavior and heat transfer features during the melting process in an STHX; and it was observed that at the end of the process, the average temperature and heat transfer rate increases by increasing the eccentricity in 0.25, 0.5 and 0.75 while the melting time decreases to 33, 57 and 64%, respectively.

Also, various research works have been conducted on STHX to fulfill the need for higher heat transfer performance and optimization by using the Kern method and Delaware method together with other approaches. Geete *et al.* (2018) analyzed the thermodynamic properties using the Kern method and found out that when the hot fluid temperature increases, the amount of entropy production, the effectiveness ratio and the transfer unit ratio declined while the heat transfer coefficient increase and pressure drop. Also, Jafari *et al.* (2018) designed and evaluated the applications of STHX of liquid food products from nanofluid thermal processing by using the Kern method, the result showed high overall heat transfer coefficients achieved with suitable linear and mass velocity. Moreover, Yousufuddin *et al.* (2018) designed and optimized STHX for cooling lean diethanolamine with different baffle spacing arrangements using the Kern method. The results on the shell side declared that increasing baffle spacing decreases the heat transfer coefficient and increases the pressure drop. Ruiz *et al.* (2018) analyzed the influence of the mass flow in an STHX in the tube side using kerosene as working fluid; the results describe that the increase in shell side mass flow rises the overall heat transferred while increase in tube side mass flow declines the pressure drop.

Finally, solar radiation could be converted through two main techniques; solar thermal collector and photovoltaic, whereby both techniques are used to minimize electric energy consumption and enhance distillation capacity to overall 67.6% efficiency when integrated with conventional desalination unit. Basin type solar still has been used as a passive solar desalinator combined with flat plat thermal collector provide efficiency 30 to 45% which shows low water production due to condensation takes place in the basin that makes it difficult to raise in evaporation temperature. In the case of spray flash desalination, the nozzles are used to disintegrate and disperse a continuous liquid phase into the chamber and cause phase change with no boundary between mass and heat transfer. In spray flash desalination things are different from basin type, here the evaporation process takes place in different units separate from the condensation unit. The evaporation unit used to get support from the solar collector, while an evacuated tube collector provides a higher indicative temperature 50 to 200^{o}C and performs well than a flat plate with indicative temperature 30 to 80^{o}C when integrated with different solar desalination systems. Shell-and-tube heat exchanger may be used as the condensation unit instead of conventional condensers due to its capacity to provide high heat transfer area to weight and volume, simply constructed in the extensive range of size depends on heat transfer and pressure drop performance. However, most of the literature explains the improvement of some parts in evaporation unit and not condensation unit such as droplet analysis, characteristics of superheated water jets, diffusion-controlled evaporation, predict the performance of spray

evaporator, the influence of the direction of injection, the flash recovery system and optimize the design as detail explained in the literature section. The current study based on optimizing the condensation unit by replacing with the shell-and-tube heat exchanger (STHX) to enhance the performance of a spray flash evaporation integrated with an evacuated tube desalination system by analyzing the effect of some parameters and configuration on the spray flash evaporator performance, and to assess the heat transfer phenomena due to mass flow rate, tube length and diameter in the design of STHX.

CHAPTER THREE

MATERIALS AND METHODS

3.1 Modification of Current System Configuration

Figure 4 illustrates the current layout which comprises several electric components namely, blower, feed pump and filter with a suction fan, water circulation pump and condenser with a fan. These components make a high level of energy intensity. Here source water from the source chamber pumped into the flash chamber via nozzles. The sprayed flash occurred and absorbs the thermal energy in the flash chamber to form steam. The thermal energy is formed through passive solar heating systems by taking advantage of the sun's free, renewable energy in the flash chamber to form steam the same way as in the basin type desalination system since our evaporation chamber is made by glazing material. Steam is escaping the chamber by passing between the chamber's walls, sucked through filter suction fan direct to the filter, then sucked by condenser suction fan and condensed, and finally stored as freshwater in a distillate reservoir. The steam is condensed when the cold water is circulated in the condenser from the water circulator tank via a second feed pump which consumes about 5.968 kWh of electric energy per operation. At the same time, the condenser suction fan sucks the steam from the filter to speed up the process in which much steam is allowed to escape. Both condenser and filter suction fans increase energy consumption on the system by 2.888 kWh and make the 8.856 kWh total energy consumption in the condensation unit. Hence, the current system energy is consumed 14.824 to19.544 kWh in a single day of operation depend on the use of four blowers which consume about 4.720 kWh.

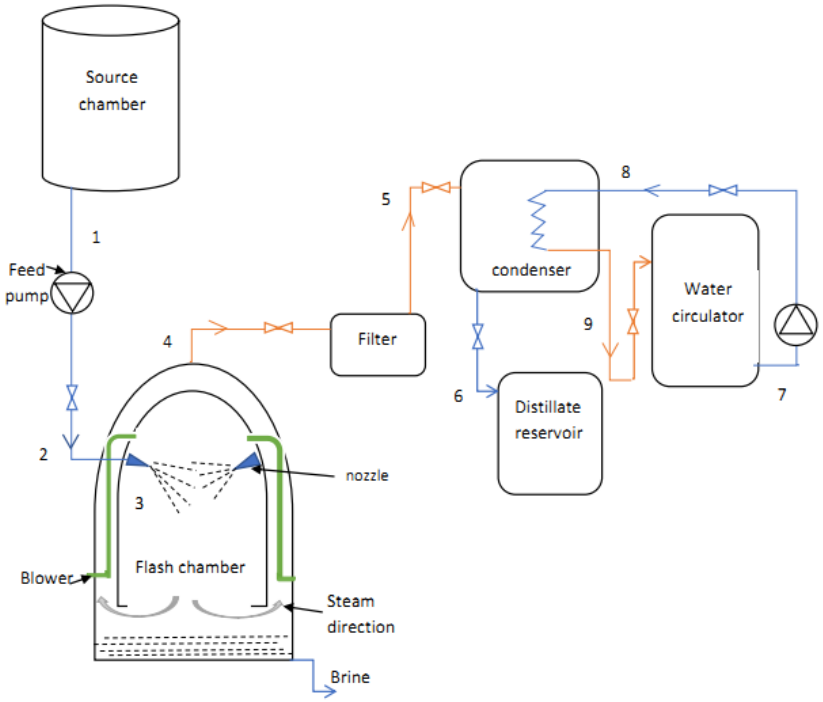

Figure 4: The current layout of the spray flash evaporation system

Figure 5 shows a schematic of a proposed layout that remains with the blower and the feed pump only which may alleviate the energy consumption through the implementation of the heat exchanger as a condensation unit. Now source water from source chamber pumped to evacuated tube collector through the heat exchanger then feed to a flash chamber via nozzles. As usual, the sprayed flash occurred and absorbs the thermal energy in the flash chamber to form steam. Steam is escaping the chamber bypassing at the top, condensed by exchanging heat with cold water from the source at the heat exchanger and stored as freshwater. The blower is embedded with the flash chamber to compress the water vapor/steam to raise its pressure and temperature (Xu *et al.*, 2019). The heat exchanger condenses outgoing steam which saves about 8.856 kWh that is consumed by the current condensation unit, at the same time becomes a preheater for the incoming cold water. The evacuated tube collector (also a preheater) raises further the temperature of the feed-water before it is fed into the flash chamber. Therefore, the proposed layout single day of operation will consume 5.968 to 10.688 kWh electric energy depend on the use of blowers.

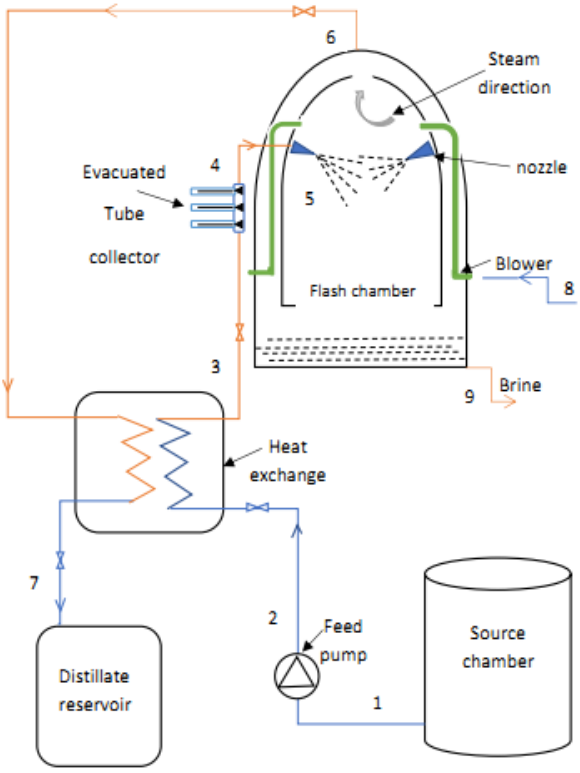

Figure 5: Proposed layout of the spray flash evaporation system

3.2 Specifying Physical Parameters

Thermal conductivity, density, viscosity and specific heat capacity of the cold and hot fluid stream were among the factors assessed at point number 6 in Fig. 5 in the primary stage in the STHX design as can be seen in Table 2, taken from the existing evaporator appeared in Fig. 6a. Double shell passes were taken into account and a triangular pitch of 1.25 space between tube to tube centers, was considered for the analysis. A single segmental baffle was chosen for ease of maintenance and high thermal features. U-tube (tube sheet) was used to permit a distinction of thermal expansion. Moreover, the outlet temperatures 29 and 28^{o}C (t_7 and t_3) for steam and water respectively were assumed to control the output and easy computation as shown in Fig. 6b. Delaware method is referred to as ideal tube bank correction that dividing the flow of fluid in the shell into many individuals steams. The method used to evaluate the effect of mass flow rate on the pressure drop, heat transfer coefficient, overall heat transfer coefficient, over-surface and over-design through equation 1 to 22.

Table 2: Physical parameters of steam and water were taken from the steam evaporator

System components	$\dot{m}$ (kg/s)	T_{inlet} (^oC)	T_{outlet} (^oC)	ρ (kg/m^3)	C_p (kJ/kg K)	μ (Pa s)	k (W/m K)	$R_{fouling}$ (m^2 K/W)
Steam	0.1-0.8	25	28	996.4	4179	0.00089	0.597	0.00018
Water		0.024	60	29	0.191	1914	0.000011	0.023	0.00009

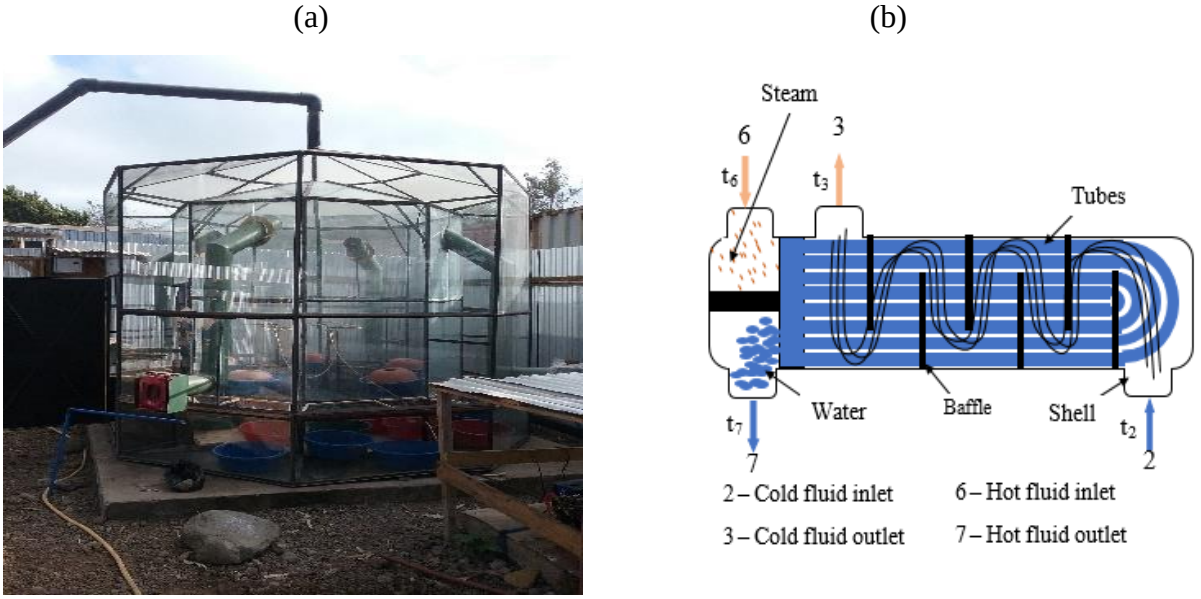

Figure 6: (a) Low-temperature evaporator in Arusha Technical College, Tanzania (b) heat exchanger model

3.3 Shell-and-Tube Heat Exchanger Design Equations

The thermal calculations of the STHX device were performed by using the essential equations found in Sections 3.3.1-3.3.6, as described in the literature (Gonçalves *et al.*, 2019).

3.3.1 Thermal Evaluation

The sensible heat transfer rate for STHX is defined by the temperature difference on the shell-side or that of the tube-side and their load was calculated using equation 1:

$$Q = \dot{m}_f Cp_f \left(t_3 - t_2\right) = \dot{m}_g Cp_g \left(t_6 - t_7\right) \quad (1)$$

Where $\dot{m}_g$ and $\dot{m}_f$ are mass flow rate of steam and water respectively, Q is heat transfer rate, Cp_g and Cp_f are specific heat capacity of steam and water respectively, t_3 and t_2 are an outlet and inlet water temperature, t_7 and t_6 are outlet and inlet temperature of steam respectively.

Equation 2 computes a logarithmic mean temperature difference (ΔT_{lm}) that used in estimating the true temperature difference in equation 3 by applying a correction factor (F_t) to allow for the departure from the true counter-current flow:

$$\Delta T_{lm} = \frac{(t_6 - t_3) - (t_7 - t_2)}{\ln\left(\frac{t_6 - t_3}{t_7 - t_2}\right)} \tag{2}$$

$$\Delta T_m = F_t \Delta T_{lm} \tag{3}$$

3.3.2 Overall Heat Transfer Coefficient Assessment

An estimated overall heat transfer coefficient (U_o) is used to attain a preliminary appraisal for the size of the STHX. According to the working fluid, the range is 1500 - 4000 W/m^{2}K as stated by Goswami (2004):

$$A = \frac{Q}{U_o \Delta T_m} \tag{4}$$

Where ΔT_m is the true temperature difference, U_o is the pilot overall heat transfer coefficient, Q is the heat transfer rate and A is a heat transfer area.

3.3.3 Tube-Side Calculations

Empirical equation 6 below was used to determine the bundle diameter. The n_1 and K_1 in the equation are coefficients determined by the tube layout and the number of tube passes from Table 3 for triangular pitch and square pitch. The number of the tubes of (n_t) is the ratio of total heat transfer area (A) and the tube outer surface area (A_t) as shown in equation 5.

$$n_t = \frac{A}{A_t} \tag{5}$$

$$D_b = d_o \left(\frac{n_t}{K_1}\right)^{\frac{1}{n_1}} \tag{6}$$

Table 3: Coefficients n1 and K1 (Towler & Sinnott, 2012)

Tube passes	1	2	4	6	8
Square pitch					
n_1	2.207	2.291	2.263	2.617	2.643
K_1	0.215	0.156	0.158	0.0402	0.0331
Triangular pitch					
n_1	2.142	2.207	2.285	2.499	2.675
K_1	0.319	0.249	0.175	0.0743	0.0365

The heat transfer coefficient (h_t) of the hot fluid stream was determined by using equation 7 below. Where, k_g is a hot fluid thermal conductivity, d_i is a tube inner diameter, Pr_t is a tube side Prandtl number 0.975, Re_t is tube side Reynolds number 1.825 x 10^5 and the flow is turbulent, μ_g and μ_w are hot fluid and water viscosity respectively:

$$h_t = \frac{k_g}{d_i} \mathrm{Re}_t^{0.8} \mathrm{Pr}_t^{0.33} \left(\frac{\mu_g}{\mu_w} \right)^{0.14} \tag{7}$$

3.3.4 Shell-Side Equations

In the following equations, D_s is a shell diameter, D_c is a clearance between a tube bundle diameter D_b and the diameter of the shell. While c_1 and m_1 are empirical coefficients presented in Table 4 that relate to the head type designed in the STHX.

$$D_s = D_c + D_b \tag{8}$$

$$D_c = c_1 + m_1 D_b \tag{9}$$

Table 4: Coefficients c_1 and m_1 (Khalfe *et al.*, 2011)

Head Type	c_1	m_1
Outside Packed Head	0.038	0.0
Pull Through Floating Head	0.0862	0.009
Split Ring Floating Head	0.0446	0.027
U-Tube or Fixed Head	0.008	0.01

Equation 10 determines the heat transfer coefficient (h_s) on the shell. Where, k_f is a shell-side thermal conductivity, d_e is a shell equivalent diameter, Pr_s is a shell side Prandtl number, J_h is a Colburn factor, μ_f, and μ_w are cold fluid and water viscosity respectively.

$$h_s = \frac{k_f}{d_e} J_h \mathrm{Pr}_s^{0.33} \left(\frac{\mu_f}{\mu_w} \right)^{0.14} \tag{10}$$

3.3.5 Overall Coefficients Calculations

Equation 11 was used to determine the required overall heat transfer coefficient, U_{req}.

$$U_{req} = \frac{Q}{\pi n_t d_o l_t \Delta T_m} \tag{11}$$

Equation 12 was used to calculate the clean-overall heat transfer coefficient, U_c.

$$U_c = \left(\frac{d_o}{h_t d_i} + \frac{d_o \ln\left(\frac{d_o}{d_i}\right)}{2k} + \frac{1}{h_s} \right)^{-1} \tag{12}$$

If $U_{req} < U_c$, the following step was considered.

Equation 13 was used to compute the design overall heat transfer coefficient:

$$U_d = \left(\frac{d_o}{h_t d_i} + \frac{d_o \ln\left(\frac{d_o}{d_i}\right)}{2k} + \frac{1}{h_s} + \frac{R_v d_o}{d_i} + R_f \right)^{-1} \tag{13}$$

If $U_d \geq U_{req}$, the next step was worthy to be carried out.

Over-design is computed in equation 14. The final design safety margin is provided by over-design in which the required fouling compensation is represented. Over-surface deals with exchanger surface area and depends on the wall and film resistances and fouling allowance, it can be obtained through equation 15.

$$O_{des} = \frac{U_d}{U_{req}} - 1 \tag{14}$$

$$O_{sur} = \frac{U_c}{U_{req}} - 1 \tag{15}$$

3.3.6 Pressure Drop Calculations

(i) Tube-Side Pressure Drop

A hot fluid pressure drop (ΔP_i) was computed as shown in equation 16. Where f_t is a Darcy friction factor, specific gravity in the tube side (s_t), tube length (l_t), hot fluid mass velocity (G_g), inner tube diameter (d_i) and n_p is a tube passes number.

$$\Delta P_i = \frac{f_t l_t G_g^2 n_p}{7.5\times10^{12} d_i s_t} \tag{16}$$

The return pressure loss was computed through equation 17:

$$\Delta P_r = 1.334\times10^{-13}(2n_p - 1.5)\frac{G_g}{s_t} \tag{17}$$

The tube side nozzles pressure drop (ΔP_{nt}) was considered through equation 18. Where G_{nt} is a tube side nozzles mass velocity and n_s is the number of tube passes.

$$\Delta P_{nt} = 2.0\times10^{-13}\frac{n_s G_{nt}^2}{s_t} \tag{18}$$

Equation 19 evaluates the overall pressure drop (ΔP_t) across the hot fluid stream on the tube side as presented below:

$$\Delta P_t = \Delta P_i + \Delta P_r + \Delta P_{nt} \tag{19}$$

(ii) Shell-Side Pressure Drop

Equation 20 evaluates initial pressure loss (ΔP_o) in the shell side. Where s_s is specific gravity, friction factor (f_s), equivalent diameter (d_e), baffle number (n_b) and D_s is a shell diameter.

$$\Delta P_o = \frac{f_s (G_g)^2 D_s (n_b + 1)}{7.5\times10^{12} d_e s_s} \tag{20}$$

Also, the pressure loss in the shell side nozzles (ΔP_{ns}) was considered through equation 21 shown below. Where G_{ns} is a shell side nozzles mass velocity and n_s is the number of tube passes.

$$\Delta P_{ns} = 2.0\times10^{-13}\frac{n_s G_{ns}^2}{s_s} \tag{21}$$

Then, the net pressure drop (ΔP_s) across the cold fluid stream on the shell side was computed by adding the nozzles pressure loss and initial shell side pressure losses as per equation 22:

$$\Delta P_s = \Delta P_o + \Delta P_{ns} \tag{22}$$

CHAPTER FOUR

RESULTS AND DISCUSSION

4.1 Effect of Mass Flow Rate on the Pressure Drop and the Heat Transfer Coefficient

Figures 7(a-c) shows the pressure drop together with heat transfer coefficient variations within the STHX with the length of 600 mm, 800 mm and 1000 mm for three different tube outer diameters of 14 mm, 12 mm and 10 mm with 1 mm thickness for each respectively through a given range of mass flow of 0.1 to 0.8 kg/s. From Fig. 7 (a-c) it can be seen that both the heat transfer coefficient and the pressure drop increase proportionally to the mass flow rate by considering the nine configurations of heat exchangers. Also, confirm that the heat transfer coefficient is much greater at any point in the range of mass flow rate compared to the pressure drop. Hence it is noted that the diameter of 10 mm shows the greatest heat transfer coefficient of 18 162, 20 881 and 23 212 W/m^2K and the maximum pressure drop of 0.328, 0.593 and 0.957 Pa. While the diameter of 14 mm shows a minimum pressure drop of 0.117, 0.223 and 0.370 Pa and a lesser heat transfer coefficient of 13 265, 15 326 and 17 107 W/m^2K in the length of 600 mm, 800 mm and 1000 mm, respectively.

Figure 7(d) illustrates the variation of the all minimum pressure drop (blue) which appears in the tube with a diameter of 14 mm versus the cold fluid stream mass flow rate in the shell side for the three different tube length exchangers. The results show that the tube configuration with a minimum length (600 mm) has a minimum pressure drop of 0.117 Pa corresponding to the rest of the configurations. Figure 4d also shows the results of the variation of the maximum heat transfer coefficient (black) which appears in the tube with a diameter of 10 mm versus cold stream mass flow rate in the shell side for the three different tube length exchangers, thus the tube configuration with a maximum length of 1000 mm portrays maximum heat transfer coefficient of 23 212 W/m^2K compared to the rest configurations.

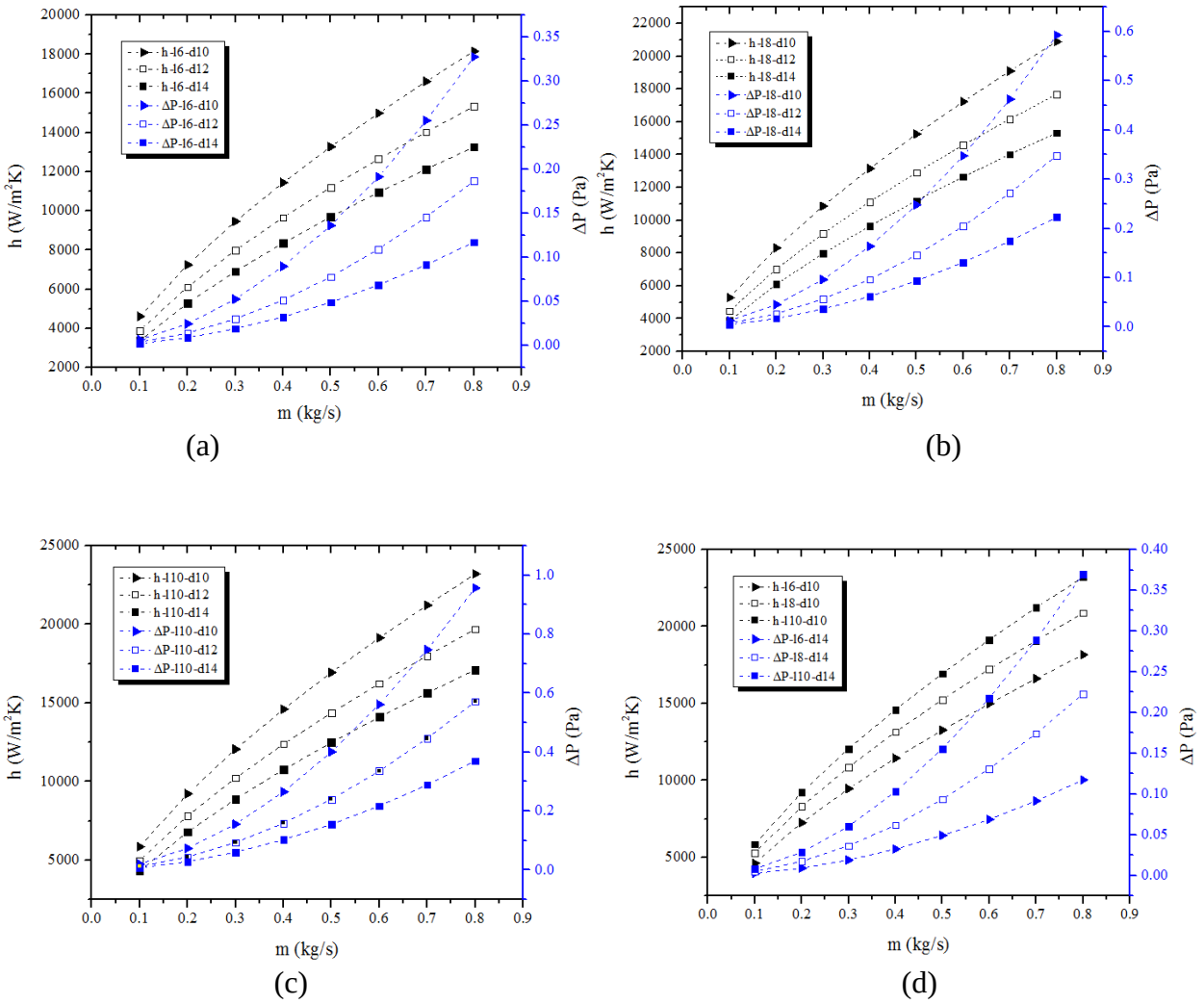

Figure 7: Pressure drop and heat transfer coefficient against mass flow rate (a) 600 mm length (b) 800 mm length (c) 1000 mm length (d) minimum pressure drop and maximum heat transfer coefficient

4.2 Effect of Mass Flow Rate on the Ratio of Heat Transfer Coefficient and Pressure Drop

Figures 8(a-c) represents the ratio of heat transfer coefficient and pressure drop (h/p) variations within the STHX with the length of 600 mm, 800 mm and 1000 mm for three different tube outer diameters of 10 mm, 12 mm and 14 mm respectively; with 1 mm thickness for each through a given range of mass flow rate 0.1 to 0.8 kg/s. It can be seen that the ratio decreases as the mass flow rate increases in all nine (9) configurations. The slope was found to be very steeper at 0.1 to 0.3 kg/s mass flow rate and becomes moderate as the mass flow rate increases. Then at the 0.1 to 0.8 kg/s flowrate, the shortest tube with a 14 mm diameter displays a high heat transfer coefficient, 1 358 087 to 113 046.2 W/m^2 K per pressure drop. While the longest tube with a 10 mm diameter has a low heat transfer coefficient, 286 708.9 to 24 258.03 W/m^2 K per pressure.

Figure 8(d) shows the maximum ratio of the heat transfer coefficient and pressure drop appears to be maximum in tubes with a 14 mm diameter for the three different length heat exchangers configurations. It can also be seen that the tube configuration with a minimum length (600 mm) has a maximum ratio compared to the rest of the configurations. Moreover, from Fig. 8c one can note the minimum ratio (black) which appears in tubes with the smallest diameter of 10 mm for the heat exchangers configuration of 1000 mm length. This does not compromise what was portrayed before to have a maximum heat transfer coefficient in comparison with the rest configurations in Fig. 7d. Here, the fact is the heat transfer coefficient is affected by pressure drop along the path and both go proportional to the mass flow. But the ratio decrease with an increase in mass flow rate.

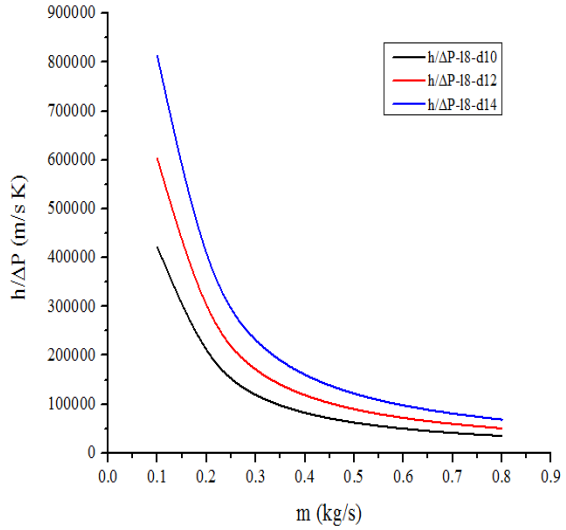

(a)

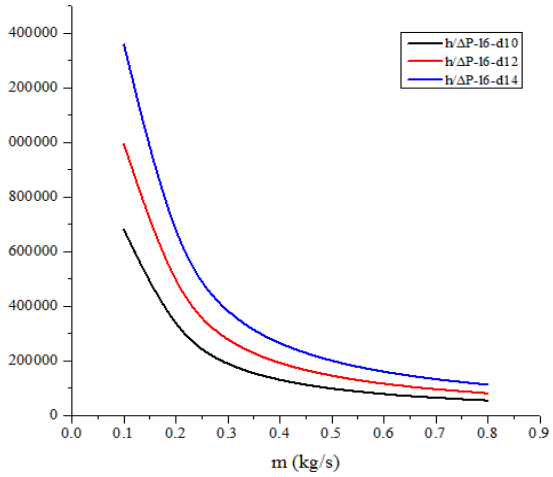

(b)

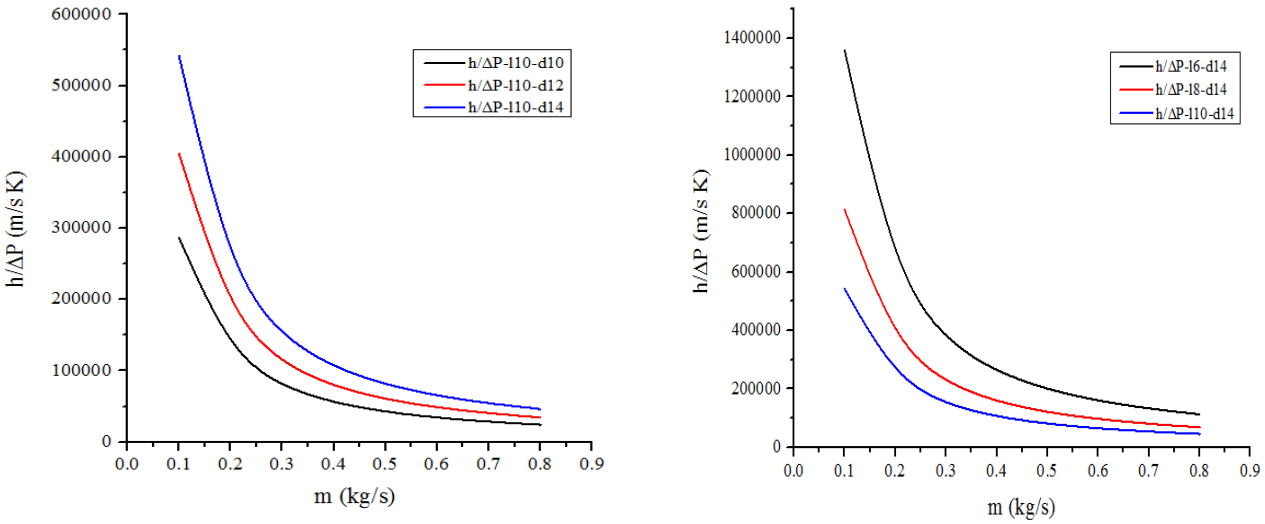

(c) (d)

Figure 8: The ratio of heat transfer coefficient and pressure drop against mass flow rate (a) 600 mm length (b) 800 mm length (c) 1000 mm length (d) maximum ratio

4.3 Effect of Mass Flow Rate on the Overall Heat Transfer Coefficient

Figures 9(a-c) expresses the effect of mass flow rate on the overall heat transfer coefficients of design heat transfer coefficient (U_d) and clean heat transfer coefficient (U_c) within the STHX with the length of 600 mm, 800 mm and 1000 mm for three different tube outer diameters of 10 mm, 12 mm and 14 mm respectively; with 1 mm thickness for each. The results for both U_d and U_c coefficients demonstrate that when the cold fluid flows over the whole surface of the shell was varied, the U_d and U_c increase constantly at any rate regardless of the difference in the tube configuration throughout the study. On the other hand, the U_c is shown to increase twice or more to that U_d when an increase in mass flow in the shell side. This is due to the significant effect of the fouling factor of the working fluids. However, the increase in mass flow and sustaining the temperatures keep U_d and U_c rising proportionally, the design coefficient is used rather than the clean coefficient based on the interest of over-design. The highest and smallest values of U_d appeared in 10 and 14 mm tube diameter, respectively.

Figure 9(d) illustrates the U_d which appears through all-tube configurations. The result shows that the tube configuration with a maximum length (1000 mm) has maximum U_d compare to the other configurations. Moreover, it can be seen that as the length of the tube increases with a decrease in diameter the maximum U_d is achieved. To provide the required rate of heat transfer the value of the U_d, should be greater than or equal to the value of the required coefficient, U_{req}. The results show that the suitable mass flow of 0.3 to 0.8 kg/s with a range of 2306 to 2539 W/m^{2}K can be selected for the proper design of the exchanger as shown in Fig. 10d.

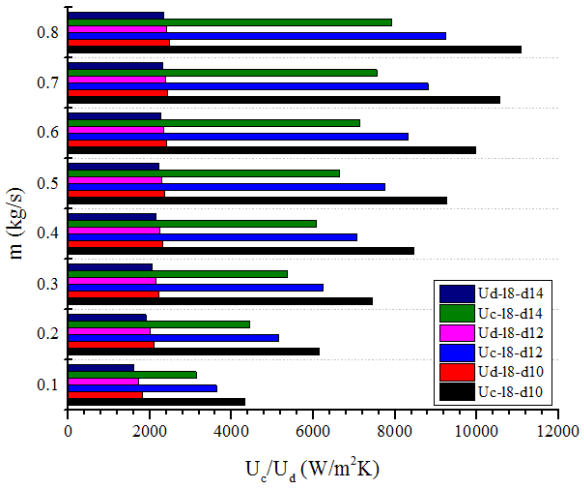

(a)

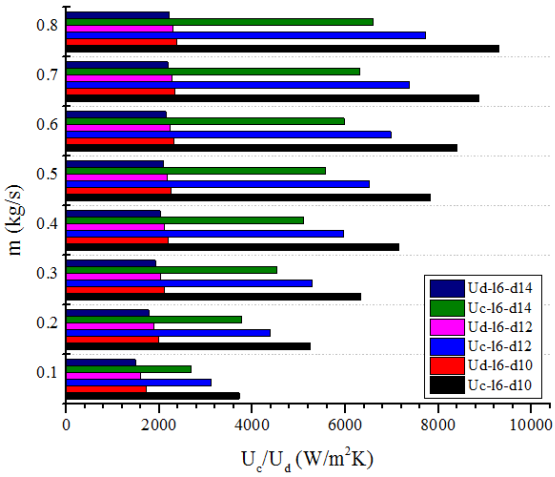

(b)

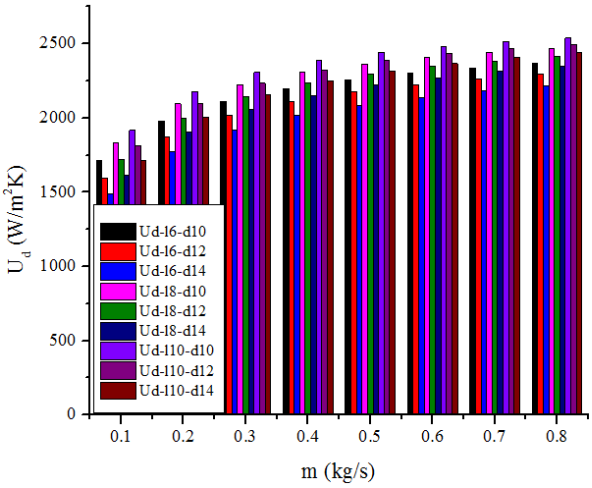

(e)

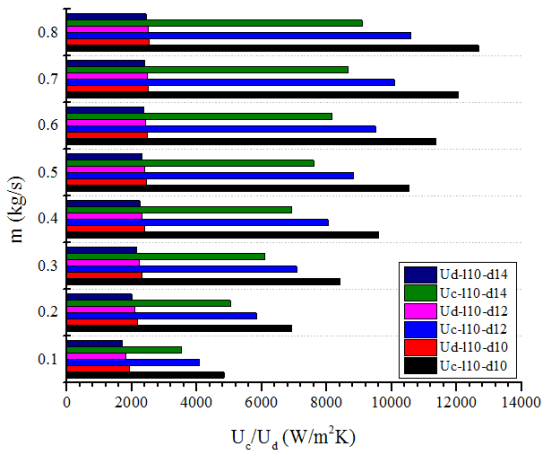

(d)

Figure 9: Overall heat transfer coefficient versus mass flow rate (a) 600 mm length (b) 800 mm length (c) 1000 mm length (d) design overall heat transfer coefficient among all configurations

4.4 Effect of Mass Flow Rate on the Over-Surface and Over-Design

Figures 10(a-c) demonstrate the over-surface (O_{sur}) and over-design (O_{des}) changes when designing the STHX with the length of 600 mm, 800 mm and 1000 mm for three different tube outer diameters of 10 mm, 12 mm and 14 mm with 1 mm thick for each respectively through a given range of 0.1 to 0.8 kg/. Since the U_{req} is much smaller than that of the U_c, the O_{sur} appeared to increase in the range of 19.2 to 463.3 as the mass flow increases. The O_{des} were shown to increase slightly from the negative value on 0.1 to 0.3 kg/s to a positive value on 0.4 to 0.8 kg/s in a range of -33.9 to 12.8.

Since engineers do recognize that there will be uncertainties in the data provided and that there may be times when the feedstock will not exactly match up to what was originally specified. A certain amount of conservatism will be required just to achieve satisfactory performance despite unforeseen circumstances. Figure 10(d) clarifies the possibility of designing the suitable STHX by displaying the greatest values of O_{des} which mostly appeared in the smallest tube diameter (10 mm) to all three tube length configurations with a total of nine samples. However, the O_{des} is a negative value at a low mass flow rate of 0.1 to 0.3 kg/s specifically to the configurations of length 600 mm and 800 mm. Conversely, as mass flow increase from 0.4 to 0.8 kg/s, the O_{des} becomes a positive value. Hereafter, the configuration with tube length 1000 mm performed well even from the mass flow of 0.3 kg/s compared to other configurations.

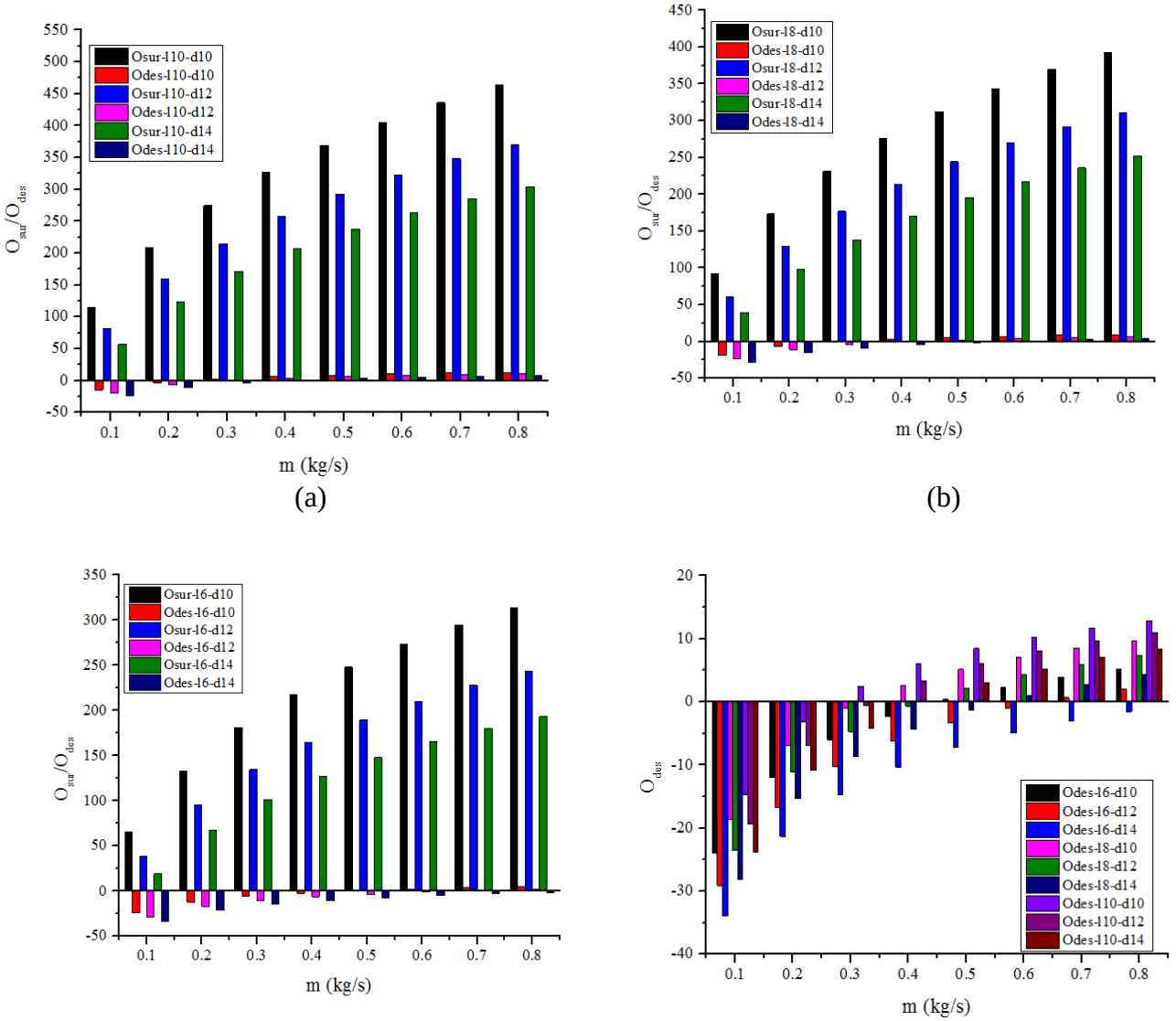

Figure 10: Over-surface and over-design versus mass flow rate (a) 600 mm length (b) 800 mm length (c) 1000 mm length (d) over-design among all configurations

CHAPTER FIVE

CONCLUSION AND RECOMMENDATIONS

5.1 Conclusion

A heat exchanger model for a low-temperature desalination system was established through the influence tube length and diameter, and mass flow rate on pressure drop, heat transfer coefficient, overall heat transfer coefficient, over-surface and over-design. After analyzing these heat transfer perimeters the following summarized conclusions were obtained. Both the heat transfer coefficient and the pressure drop increase proportionally to the mass flow rate among all nine configurations of heat exchangers. But the pressure drop is noticed to be very low 0.328 to 0.957 Pa for all studied configurations that will lower the pumping power. The clean overall heat transfer coefficient increases twice or more to that of the design coefficient when an increase in mass flow in the shell side due to the effect of the fouling factor. The maximum design coefficient is achieved by increasing the tube length with a decrease in diameter. Also, the mass flow of 0.3 to 0.8 kg/s is suitable for the proper design of exchanger in the present study. The configuration with the 1000 mm length and 10 mm diameter which provides high heat transfer is recommended to work with a maximum flow rate of 0.8 kg/s to achieve a maximum heat transfer coefficient of 23 212 W/m^2K, while 12.8 is a maximum over-design coefficient achieved on 0.8 kg/s mass flow. The energy-saving of the proposed system is about 8.856 kWh as the replacement of the STHX from the existing condensation unit. While the current system energy is consumed about 14.824 to 19.544 kWh in a single day of operation and is improved to the range of 5.968 to 10.688 kWh for the proposed system depend on the use of blowers which consume about 4.720 kWh in peak operation.

5.2 Recommendations

In general, the performance of the proposed layout system seems to be very suitable in terms of workflow and less energy consumption to the system. Therefore, the implementation of the proposed layout of the low-temperature desalination unit at Arusha Technical College will enhance the daily operation. Since the current research is based on numerical computation, the fabrication of STHX and pilot testing based on the proposed layout is highly recommended that will ensure the availability of enough data to compare with the existing system. Also at that moment, for prospective energy efficiency, there is amply of research to be done on the current glazing evaporator performance.

REFERENCES

Ahmed, M., Zubair, S. M., Abido, M., & Bahaidarah, H. M. (2018). An innovative closed-air closed-desiccant HDH system to extract water from the air: A case for zero-brine discharge system. *Desalination, 445*, 236-248.

Al-Kharabsheh, S., & Yogi, D. (2003). Analysis of an innovative water desalination system using low-grade solar heat. *Desalination, 156*(1-3), 323-332.

Ambekar, A. S., Sivakumar, R., Anantharaman, N., & Vivekenandan, M. (2016). CFD simulation study of shell and tube heat exchangers with different baffle segment configurations. *Applied Thermal Engineering, 108*, 999-1007.

Araghi, A. H., & Khiadani, M. (2018). Experimental investigation and analysis of a new single-stage vacuum spray flash desalinator utilising a gas-liquid ejector. *Journal of Cleaner Production, 190*, 118-127.

Arani, A. A. A., & Moradi, R. (2019). Shell and tube heat exchanger optimization using new baffle and tube configuration. *Applied Thermal Engineering, 157*, 113736.

Bichkar, P., Dandgaval, O., Dalvi, P., Godase, R., & Dey, T. (2018). Study of shell and tube heat exchanger with the effect of types of baffles. *Procedia Manufacturing, 20*, 195-200.

Cai, B., Tuo, X., Song, Z., Zheng, Y., Gu, H., & Wang, H. (2018). Modeling of spray flash evaporation based on droplet analysis. *Applied Thermal Engineering, 130*, 1044-1051.

Chen, Q., & Chua, K. J. (2018). A spray assisted low-temperature desalination technology. In V. G. Gude (Ed), *Emerging Technologies for Sustainable Desalination Handbook* (pp. 255-284): Elsevier.

Chen, Q., Ja, M. K., Li, Y., & Chua, K. (2018a). Energy, economic and environmental (3rd Ed) analysis and multi-objective optimization of a spray-assisted low-temperature desalination system. *Energy, 151*, 387-401.

Chen, Q., Ja, M. K., Li, Y., & Chua, K. (2018b). Evaluation of a solar-powered spray-assisted low-temperature desalination technology. *Applied Energy, 211*, 997-1008.

Chen, Q., Li, Y., & Chua, K. (2018). Experimental and mathematical study of the spray flash evaporation phenomena. *Applied Thermal Engineering, 130*, 598-610.

El-Agouz, S., El-Aziz, G. A., & Awad, A. (2014). Solar desalination system using spray evaporation. *Energy, 76*, 276-283.

El-Fiqi, A. K., Ali, N., El-Dessouky, H., Fath, H., & El-Hefni, M. (2007). Flash evaporation in a superheated water liquid jet. *Desalination, 206*(1-3), 311-321.

Geete, A., Patel, V., S. Tanwar, S., Kushwah, S., Lodhi, N. S., & Kushwah, V. (2018). Thermodynamic analysis of designed and fabricated shell-and tube-type heat exchanger by DSTHE software: Kern method. *International Journal of Ambient Energy, 39*(4), 343-351.

Gonçalves, C. D. O., Costa, A. L., & Bagajewicz, M. J. (2019). Linear method for the design of shell and tube heat exchangers using the Bell–Delaware method. *American Institute of Chemical Engineers Journal, 65*(8), e16602.

Goswami, D. Y. (2004). *The CRC Handbook of Mechanical Engineering*: CRC press.

Gude, V. G., & Nirmalakhandan, N. (2009). Desalination at low temperatures and low pressures. *Desalination, 244*(1-3), 239-247.

He, T. X., & Yan, L. J. (2009). Application of alternative energy integration technology in seawater desalination. *Desalination, 249*(1), 104-108.

Herrero-Gonzalez, M., Diaz-Guridi, P., Dominguez-Ramos, A., Ibañez, R., & Irabien, A. (2018). Photovoltaic solar electrodialysis with bipolar membranes. *Desalination, 433*, 155-163.

Hou, J., Yang, J., Chang, Z., Zheng, H., & Su, Y. (2018). The mass transfer coefficient assessment and productivity enhancement of a vertical tubular solar brackish water still. *Applied Thermal Engineering, 128*, 1446-1455.

Ikegami, Y., Sasaki, H., Gouda, T., & Uehara, H. (2006). Experimental study on a spray flash desalination (influence of the direction of injection). *Desalination, 194*(1-3), 81-89.

Jafari, S. M., Saramnejad, F., & Dehnad, D. (2018). Designing and application of a shell and tube heat exchanger for nanofluid thermal processing of liquid food products. *Journal of Food Process Engineering, 41*(3), e12658.

Kakaç, S., Liu, H., & Pramuanjaroenkij, A. (2002). *Heat exchangers: selection, rating, and thermal design*: CRC press.

Khalfe, N. M., Lahiri, K. S., & Wadhwa, K. S. (2011). Simulated annealing technique to design minimum cost exchanger. *Chemical Industry and Chemical Engineering Quarterly/CICEQ, 17*(4), 409-427.

Khan, M. M. A., Ibrahim, N. I., Mahbubul, I., Ali, H. M., Saidur, R., & Al-Sulaiman, F. A. (2018). Evaluation of solar collector designs with integrated latent heat thermal energy storage: A review. *Solar Energy, 166*, 334-350.

Li, C., Goswami, Y., & Stefanakos, E. (2013). Solar assisted sea water desalination: A review. *Renewable and Sustainable Energy Reviews, 19*, 136-163.

Liu, X., Chen, W., Gu, M., Shen, S., & Cao, G. (2013). Thermal and economic analyses of solar desalination system with evacuated tube collectors. *Solar Energy, 93*, 144-150.

Mahbubul, I., Khan, M. M. A., Ibrahim, N. I., Ali, H. M., Al-Sulaiman, F. A., & Saidur, R. (2018). Carbon nanotube nanofluid in enhancing the efficiency of evacuated tube solar collector. *Renewable Energy, 121*, 36-44.

Raj, A. M., Kalidasa, M. K., Rajaseenivasan, T., & Srithar, K. (2016). A review on flash evaporation desalination. *Desalination and Water Treatment, 57*(29), 13462-13471.

Miyatake, O., Tomimura, T., & Ide, Y. (1985). Enhancement of spray flash evaporation by means of the injection of bubble nuclei, 107, 176-182.

Miyatake, O., Tomimura, T., Ide, Y., & Fujii, T. (1981). An experimental study of spray flash evaporation. *Desalination, 36*(2), 113-128.

Miyatake, O., Tomimura, T., Ide, Y., Yuda, M., & Fujii, T. (1981). Effect of liquid temperature on spray flash evaporation. *Desalination, 37*(3), 351-366.

Mutair, S., & Ikegami, Y. (2009). Experimental study on flash evaporation from superheated water jets: Influencing factors and formulation of correlation. *International Journal of Heat and Mass Transfer, 52*(23-24), 5643-5651.

Mutair, S., & Ikegami, Y. (2010). Experimental investigation on the characteristics of flash evaporation from superheated water jets for desalination. *Desalination, 251*(1-3), 103-111.

Muthunayagam, A., Ramamurthi, K., & Paden, J. R. (2005). Modelling and experiments on vaporization of saline water at low temperatures and reduced pressures. *Applied Thermal Engineering, 25*(5-6), 941-952.

Nitsche, M., & Gbadamosi, R. O. (2015). *Heat exchanger design guide: a practical guide for planning, selecting and designing of shell and tube exchangers*: Butterworth-Heinemann.

Pahamli, Y., Hosseini, M. J., Ranjbar, A. A., & Bahrampoury, R. (2016). Analysis of the effect of eccentricity and operational parameters in PCM-filled single-pass shell and tube heat exchangers. *Renewable Energy, 97*, 344-357.

Qi, C., Wang, X., Miao, C., Feng, H., & Lv, Q. (2018). Flash recovery system analysis and flashing tank optimization in desalination plants. *International Journal of Heat and Mass Transfer, 119*, 175-184.

Rahimi-Ahar, Z., Hatamipour, M. S., & Ghalavand, Y. (2018). Solar assisted modified variable pressure humidification-dehumidification desalination system. *Energy Conversion and Management, 162*, 321-330.

Rajaseenivasan, T., & Srithar, K. (2017). Potential of a dual purpose solar collector on humidification dehumidification desalination system. *Desalination, 404*, 35-40.

Roy, R. (2018). Optimization of design parameters on shell and tube heat exchangers using flower pollination algorithm based on economic dispatch. *International Journal for Emerging Research and Development, 1*(5), 11-15.

Ruiz, L. D., Peñaloza, C. A., & Ochoa, G. V. (2018). Effect of the Mass Flow Rate on the Heat Transfer Phenomena in a Shell and Tube Heat Exchanger. *International Journal of Applied Engineering Research, 13*(14), 11387-11391.

Sharon, H., & Reddy, K. (2015). A review of solar energy driven desalination technologies. *Renewable and Sustainable Energy Reviews, 41*, 1080-1118.

Siddique, M., Turkmen, N., Al-Rabghi, O. M., Shabana, E., & Albeirutty, M. H. (2018). Small-scale low pressure 'single effect distillation' and single stage flash'solar driven barometric desalination units: A comparative analysis. *Desalination, 444*, 53-62.

Solanki, A. K., & Kumar, R. (2018). Condensation of R-134a inside dimpled helically coiled tube-in-shell type heat exchanger. *Applied Thermal Engineering, 129*, 535-548.

Somasekhar, K., Rao, K. M., Sankararao, V., Mohammed, R., Veerendra, M., & Venkateswararao, T. (2018). A CFD investigation of heat transfer enhancement of shell and tube heat exchanger using Al_2O_3-water nanofluid. *Materials Today: Proceedings, 5*(1), 1057-1062.

Stengler, J., Schaber, K., & Mall-Gleissle, S. (2018). Experimental study on low temperature desalination by flash evaporation in a novel compact chamber design. *Desalination, 448*, 103-112.

Sundén, B., & Manglik, R. M. (2007). *Plate heat exchangers: design, applications and performance*. Wit Press.

Thakur, G., Singh, G., Thakur, M., & Kajla, S. (2018). An Experimental Study of Nanofluids Operated Shell and Tube Heat Exchanger with Air Bubble Injection. *International Journal of Engineering, 31*(1), 136-143.

Thulukkanam, K. (2013). *Heat Exchanger Design Handbook*: CRC press.

Towler, G., & Sinnott, R. (2012). *Chemical Engineering Design: Principles, Practice and Economics of PLant and Process Design*: Elsevier.

Wang, R., & Ge, T. (2016). *Advances in Solar Heating and Cooling*: Woodhead Publishing.

Wang, R., Xu, Z., & Ge, T. (2016). Introduction to solar heating and cooling systems. *Advances in Solar Heating and Cooling* (pp. 3-12): Elsevier.

Wellmann, J., Neuhäuser, K., Behrendt, F., & Lehmann, M. (2015). Modeling an innovative low-temperature desalination system with integrated cogeneration in a concentrating solar power plant. *Desalination and Water Treatment, 55*(12), 3163-3171.

Xu, H., & Dai, Y. (2019). Parameter analysis and optimization of a two-stage solar assisted heat pump desalination system based on humidification-dehumidification process. *Solar Energy, 187*, 185-198.

Xu, H., Sun, X., & Dai, Y. (2019). Thermodynamic study on an enhanced humidification-dehumidification solar desalination system with weakly compressed air and internal heat recovery. *Energy Conversion and Management, 181*, 68-79.

Yousufuddin, S., Al-Bazzaz, M., Al-Zurayqi, M., & Al-Yami, F. (2018). Design and Optimization of a Shell and Tube Heat Exchanger with Different Baffle Spacing Arrangement for Cooling Lean Diethanolamine. *SciFed Journal of Chemical Research, 2*(1), 1-10

Zhao, L., Wang, M., Wang, P., Zhu, X., Qiu, Q., & Shen, S. (2018). SSExperimental Study on the Internal Flow Field and Spray Characteristics of Hollow Nozzle. *Applied Thermal Engineering*.

Zheng, H. (2017). *Solar Energy Desalination Technology*: Elsevier.

RESEARCH OUTPUTS

(i) Research paper accepted in Paddy and Water Environment Journal.

(ii) Poster Presentation